ChemComm

COMMUNICATION

View Article Online
View Journal | View Issue

Cite this: *Chem. Commun.*, 2024, **60**, 11936

Received 12th July 2024,
Accepted 23rd September 2024

DOI: 10.1039/d4cc03488k

rsc.li/chemcomm

Dye self-organization in doped silica nanoparticles increases the electrochemiluminescence emission in magnetic bead-based assays†

Yematawa Addis Alemu,‡ Marinella Difonzo,‡ Damiano Genovese, Francesco Paolucci, Luca Prodi, Enrico Rampazzo* and Giovanni Valenti*

We have investigated the effect of dye distribution on the electrochemiluminescence (ECL) intensity measured with a simplified magnetic bead-based immunoassay for two families of silica nanoparticles (NPs) doped with the cationic $Ru(bpy)_3^{2+}$ and the zwitterionic $Ru(bpy)_2bps$ complexes (bps = bathophenanthroline disulfonate). The NPs doped with the $Ru(bpy)_2bps$ complex, which can efficiently self-organize in the NP volume favoring ECL generation, resulted in 150–400% signal enhancement compared to the $Ru(bpy)_3^{2+}$-doped ones.

Electrochemiluminescence (ECL) has been largely explored as a powerful bioanalytical tool for the determination of various bioanalytes in complex matrices. It is based on the application of electric potential at the surface of an electrode; the subsequent formation of redox-active species, through a series of electron transfer reactions, generates luminophores in a light-emitting excited state. ECL benefits from an outstanding signal-to-noise ratio compared to photoluminescence, with minimized background luminescence and scattering signals leading to high sensitivity and extremely low detection limits.[1,2] Considering these advantages and its wide dynamic range, ECL bioanalytical applications in aqueous environments have rapidly increased through the years since the discovery of sacrificial co-reactants as redox shuttles to trigger emission from derivatives of $Ru(bpy)_3^{2+}$ (tris(2,2′-bipyridyl)ruthenium(II)) complexes. A co-reactant is in most cases a molecular species that can be reduced or oxidized in the water potential window, producing radicals reacting with the emitter molecule leading to the formation of its excited state. The most successful emitter/co-reactant couple to date is the $Ru(bpy)_3^{2+}$/TPrA (tri-*n*-propylamine) one, which is involved in a heterogeneous oxidative–reduction mechanism also called the remote ECL mechanism.[3] This ECL mechanism has led to the commercialization of a variety of technologies, including Elecsys® developed by Roche Diagnostics and Hitachi. Since ECL emission is limited by the diffusion of the co-reagent reactive intermediates that occur within a few micrometers outside of the electrode surface, most ECL biosensors are based on antibody sandwich assays built on the electrode surface or more often with magnetic microbead (MMB) technology, which offers straightforward integration and adaptability of the same microfluidic device to a huge number of different immunoassays (Fig. 1). In this last configuration, antibodies are usually linked to the surface of MMBs to capture the analyte that is finally recognized by a second luminophore(s)-labeled recognition antibody. MMBs are held by a magnetic field on the electrode surface inside an ECL electrochemical cell, and this strategy facilitates the concentration of the analyte to the electrode surface, the washing procedures, and the recycling of the same electrode, reducing the cost and time of the analysis. Strategies to increase the ECL emission with alternative labels have been focused on the development of quantum dots (QDs),[4–6] dye-doped silica nanoparticles (DDSNPs),[7–9] and carbon nanodots.[10] Among these, DDSNPs are intriguing systems allowing

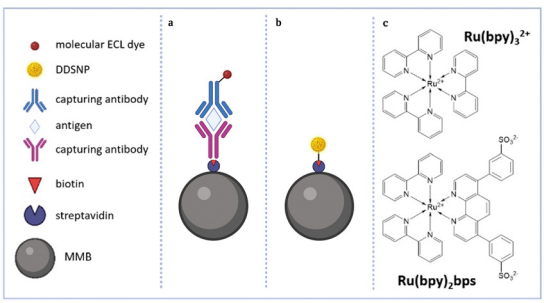

Fig. 1 (a) Schematization of a MMB-based immunoassay with an antibody labelled by molecular ECL emitter; (b) simplified immunoassay model based on MMBs used in this work to test the ECL performances of DDSNPs; (c) molecular structures of the $Ru(bpy)_3^{2+}$ and $Ru(bpy)_2bps$ dyes.

Dipartimento di Chimica, Giacomo Ciamician – Via F. Selmi 2, 40126 Bologna, Italy. E-mail: enrico.rampazzo@unibo.it, g.valenti@unibo.it

† Electronic supplementary information (ESI) available. See DOI: https://doi.org/10.1039/d4cc03488k

‡ Yematawa Addis Alemu, and Marinella Difonzo contributed equally to this work.

the organization of a high number of active dyes in a single site,[11] leading to large signal amplifications if compared to molecular dyes. The inclusion of dyes in DDSNPs can be obtained by covalent inclusion of water-soluble alkoxysilane functionalized dyes or through physical entrapment driven by electrostatic interactions between silica and the positively charged luminescent molecules. The DDSNP silica matrix provides a UV-vis transparent, rigid and inert environment for the embedded dyes, and their surface chemistry can be tailored for bioconjugation and colloidal stabilization.[12] ECL nanoprobes, primarily doped with $Ru(bpy)_3^{2+}$ and its derivatives, were shown to detect extremely low levels of biomarkers, even in complex systems.[9,13] However, there is still a scarcity of investigations to elucidate how the ECL intensity of DDSNPs is influenced by key features such as size, dye distribution and surface chemistry. In this framework, we showed how the dye charge accumulation produced by an increasing number of $Ru(bpy)_3^{2+}$ complexes in core–shell silica-PEG doped nanoparticles can be detrimental to the increase of the ECL emission, hampering the interaction between the nanoparticles and positively charged co-reagent intermediates.[14,15] It is noteworthy that self-organization of the dyes can be obtained by proper screening of the electrostatic charges with specific counterions, producing huge improvements in the performances of dye-doped nanoparticles.[16] Here, we investigate how the ECL emission intensities of silica NPs doped with two different Ru(II) polypyridyl complexes can be influenced by the self-organization of these dyes within the DDSNPs and by the NP size. For this purpose, $Ru(bpy)_3^{2+}$ and the zwitterionic $Ru(bpy)_2bps$ complex,[17] in which one bipyridine is replaced by the bathophenanthroline disulfonate ligand (bps, Fig. 1), have been used to fabricate two sets of biotinylated DDSNPs – **NPs-Ru(bpy)$_3^{2+}$** and **NPs-Ru(bpy)$_2$bps** – that have been synthesized by a reverse microemulsion (water-in-oil) method. Tetraethyl orthosilicate (TEOS) and ammonia have been used as a silica precursor and catalyst, respectively (Fig. S1, ESI†). With this strategy, the average NP size can be changed smoothly by varying the water-to-surfactant molar ratio, but keeping the other synthetic parameters constant.[18] Water-to-surfactant molar ratios of 20, 8 and 6 have been used to obtain in each set of NPs three comparable sizes of highly monodispersed and spherical NPs – named as small, medium and large, respectively. These particles – as shown by the morphological characterization performed by TEM (transmission electron microscopy) and DLS (dynamic light scattering) – show homogeneous silica core diameters spanning between 20–120 nm and hydrodynamic diameters in the 50–200 nm range, finely tuned by changing the amount of water in the reverse microemulsion (Table 1, Fig. 2 and Fig. S3–S5, ESI†). During the synthesis, the shell of these DDSNPs was enriched by organosilicon derivatives such as 3-(aminopropyl)-triethoxysilane (APTES) for biotinylation purposes and 3-(trihydroxysilyl)-propylmethylphosphonate (THPMP) to improve colloidal stability and the permeability of the shell to co-reactant molecules, and to reduce non-specific binding,[12] as shown by the low *Z*-potential values (Table 1). The two NP groups show absorption and emission spectra profiles that are very similar to those of their corresponding reference dye in water solution (Fig. S6, ESI†), meaning that the electronic ground state of the embedded luminophores is not affected by the encapsulation in the NP silica matrix. We then estimated the dye concentration for each NP suspension in water by UV-vis absorbance measurements, using the molar extinction coefficient of the Ru(II) complexes in water. The average number of Ru(II) complexes per NP was determined considering the concentration of DDSNPs measured by NTA (nanoparticle tracking analysis) measurements. The number of Ru(II) complexes per particle is in the range 7.3×10^2–7.7×10^4 dyes per NP (Table S1, ESI†). We also found that, within each set of NPs, the samples show quite similar photoluminescence quantum yields (ϕ_{PL}, Table 1), that are three or two times larger than those of their reference compound $Ru(bpy)_3^{2+}$ or $Ru(bpy)_2bps$, respectively. These results show that the Ru(II) complexes, when encapsulated in NPs, are scarcely quenched by dioxygen and that excitation and emission processes occur with a good efficiency that is not affected by NP size. We then have studied the ECL emission of the NPs in aqueous conditions under heterogeneous oxidative-reduction conditions, using TPrA as a co-reactant, with a plausible mechanism that is summarized in

Table 1 Morphological, photophysical and ECL data for the **NPs-Ru(bpy)$_3^{2+}$** and **NPs-Ru(bpy)$_2$bps** samples and the reference dyes **Ru(bpy)$_3^{2+}$** and **Ru(bpy)$_2$bps**

Samples		$d_C \pm$ SD (nm)	$d_H \pm$ SD (nm)	PDI	ζ-Pot (mV)	ϕ_{PL}	PL (a.u.)	ECL (a.u.)	τ_1 (ns); Rel. %	τ_2 (ns); Rel. %	χ^2
Ru(bpy)$_3^{2+}$		—	—	—	—	0.04	—	—	350; 100	—	1.099
NPs-Ru(bpy)$_3^{2+}$	Small	42 ± 4	85 ± 1	0.10	−20 ± 2	0.14	$(9.9 \pm 0.8) \times 10^5$	$(6.8 \pm 0.3) \times 10^5$	305; 61	645; 39	0.908
	Medium	66 ± 4	110 ± 1	0.11	−14.4 ± 0.4	0.17	$(9.4 \pm 0.8) \times 10^5$	$(2.1 \pm 0.3) \times 10^5$	285; 40	815; 60	1.175
	Large	118 ± 9	193 ± 4	0.13	−22 ± 1	0.14	$(7.9 \pm 0.9) \times 10^5$	$(6 \pm 1) \times 10^4$	285; 30	790; 70	1.092
Ru(bpy)$_2$bps		—	—	—	—	0.07	—	—	725; 100	—	1.022
NPs-Ru(bpy)$_2$bps	Small	22 ± 2	55 ± 3	0.38	−13.3 ± 0.4	0.22	$(2.0 \pm 0.1) \times 10^6$	$(2.1 \pm 0.1) \times 10^6$	730; 89	1850; 11	1.153
	Medium	88 ± 6	119 ± 2	0.15	−36 ± 2	0.14	$(1.3 \pm 0.3) \times 10^6$	$(1.18 \pm 0.07) \times 10^6$	750; 100	—	1.009
	Large	110 ± 9	146 ± 2	0.06	−28 ± 4	0.13	$(1.2 \pm 0.2) \times 10^6$	$(4.7 \pm 0.1) \times 10^5$	740; 82	3530; 18	1.134

d_c: silica core diameter (TEM); d_H: hydrodynamic diameter (DLS, water 25 °C); PDI: d_H polydispersion index; ζ-pot: zeta potential (water, 25 °C); ϕ_{PL}: photoluminescence quantum yield (water, aerated, λ_{ex} = 450 nm); PL: photoluminescence emission intensity measured by luminescence confocal microscopy analysis; ECL: emission measured by ECL microscopy; τ_i (ns), Rel. %: *i*-th excited state lifetime component and its relative population; χ^2: chi-squared test for excited-state decay fitting curves.

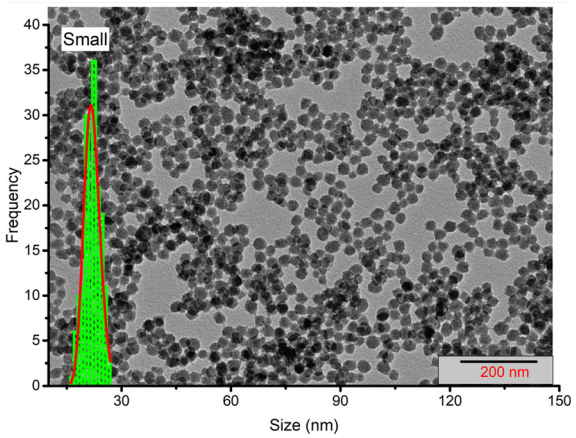

Fig. 2 TEM image and silica core diameter distribution for sample NPs-Ru(bpy)$_2$bps (small): d_c = (22 ± 2) nm. Other sample images are reported in the ESI.†

eqn (S1)–(S6) (ESI†). To compare the amount of ECL signal produced by DDSNPs during a MMB-based assay, it is important to consider that it is influenced by numerous variables. The signal intensity depends on the effectiveness of the interaction between dyes and co-reagents, and by the average efficiency with which the dyes in the DDSNPs emit. These factors depend on the kind of dye, on their position within the NP, and finally on the core–shell morphology and porosity of the NP. Another variable is represented by the total number of dyes involved in the ECL process – which normally increases by increasing the size of the NPs – but also on the capability of the NPs to densely pack on the surface of the MMB, a process that is mediated by bio-recognition events and that is expectedly more efficient for smaller NPs. For these reasons we have mimicked a MMB-based immunoassay, to measure the ECL emission of the slowly diffusing biotinylated DDSNPs, that have been coupled to streptavidine-coated MMBs of 2.8 μm diameter (Fig. S1 and S2, ESI†). Experiments were performed in a 0.2 M phosphate buffer solution containing 180 mM of TPrA at pH 6.9. ECL images were acquired by an epifluorescence microscope. This allowed the observation of the ECL emission of single MMBs to quantify the absolute ECL intensity (Fig. 3 (left) and Fig. S9, S10, ESI†). To elucidate the relationships between the size and dye distribution of the NPs on their ECL emission more quantitatively, we have normalized the absolute ECL emission of the MMB@NPs ensemble by their corresponding average photoluminescence emission intensities, which we measured using confocal imaging (Fig. 3, right). These latter intensities (Fig. S7 and S8, ESI†) represent a good estimation of the amount of dyes that are present on each MMB@NPs ensemble since the ϕ_{PL} of the different samples in each NP set is very similar (Table 1). These photoluminescence intensities were determined by confocal microscopy analysis, exciting the Ru(II) dyes at 489 nm and selecting their photoluminescence with a 595/50 nm emission filter. The ECL data – normalized per Ru(II) complex – show that the smaller NPs are more efficient ECL emitters than larger ones and that for similar sizes **NPs-Ru(bpy)$_2$bps** are more efficient ECL emitters than **NPs-Ru(bpy)$_3^{2+}$** (Fig. 3 right). This trend can be explained considering that in smaller NPs the higher surface-to-volume ratio facilitates the interaction between the Ru(II) complexes and the co-reagent intermediates and that the Φ_{PL} of the reference Ru(bpy)$_2$bps complex is larger than that of Ru(bpy)$_3^{2+}$ in aerated conditions (Table 1). Remarkably, the decrease of the ECL signal with increasing size shown in Fig. 3 is much lower for **NPs-Ru(bpy)$_2$bps** if compared to **NPs-Ru(bpy)$_3^{2+}$**, although the photoluminescence of the Ru(II) complexes in each NP set shows similar efficiencies. This means that larger **NPs-Ru(bpy)$_2$bps** are excited more efficiently during the ECL mechanism than the **NPs-Ru(bpy)$_3^{2+}$** of similar size. A reason for this can be found in a more favorable Ru(II) dye organization within the NP. Time-resolved photoluminescence measurements performed for both NP samples in aerated aqueous dispersion show in most cases two average excited state lifetime components for the Ru(II) complexes. This indicates that the dyes within the NP can be represented on average by two populations located in two different NP core districts. A first population of less bright luminophores – closer to the periphery of the core and at the boundary with the more porous organo-silica shell – that can be partially quenched by dioxygen, and that shows the shorter lifetime component τ_1; and a second population of dyes that are unaffected by dioxygen because they are more embedded in the silica matrix, that show the longer lifetime component τ_2 (Table 1). Excited lifetime data in Table 1 show how **NPs-Ru(bpy)$_2$bps** present a larger fraction of Ru(II) complexes with the shorter lifetime component τ_1 compared to **NPs-Ru(bpy)$_3^{2+}$**, and consequently the majority of Ru(II) complexes located at the periphery of the core, much closer to the more permeable organo-silica shell where the interaction with TPrA radicals is more efficient. This more detailed analysis indicates how the charge and the ligand nature of Ru(II) complexes can determine the self-organization of the luminophores within the NP silica matrix, affecting the interactions with the co-reactant intermediates. The self-organization of the Ru(bpy)$_2$bps complexes inside the **NPs-Ru(bpy)$_2$bps** is probably due to its zwitterionic nature causing some electrostatic repulsion between the negatively charged sulfonate moieties and the incipient negative charge of silica oligomers formed upon TEOS hydrolysis and condensation, that forces the complexes to locate at the periphery of the forming NP during the formation of silica. In this work, we have shown that the ECL emission intensity of luminescent silica NPs doped with the positively charged Ru(bpy)$_3^{2+}$ or the zwitterionic Ru(bpy)$_2$bps complexes is influenced by the NP size. ECL emission intensities – normalized per Ru(II) complex – are higher for NPs with smaller sizes because a higher surface-to-volume ratio increases the fraction of Ru(II) complexes that can be involved in the redox processes triggering the ECL emission. This increase overcomes the dioxygen luminescence dynamic quenching effect involving the Ru(II) complexes that is larger for smaller nanoparticles. Furthermore, a comparison between NPs of equal size shows that the ECL emission of **NPs-Ru(bpy)$_2$bps** is higher than that of **NPs-Ru(bpy)$_3^{2+}$**. This difference is not just linked to the photoluminescence

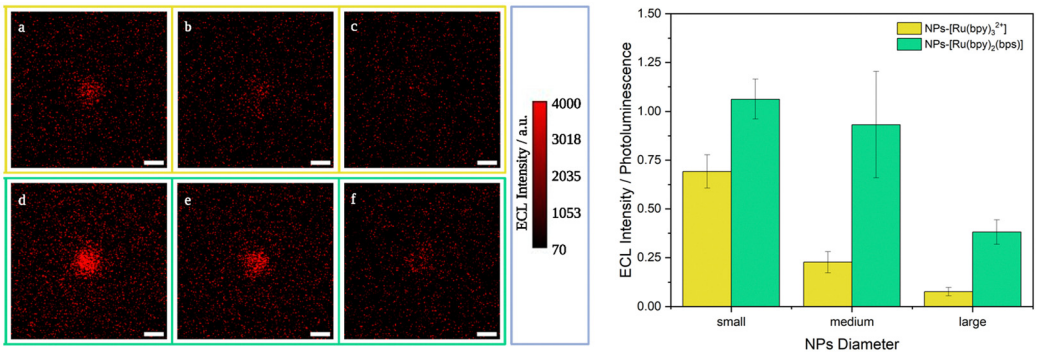

Fig. 3 Left: Representative single ECL images of 2.8 μm MMB@NPs, other images in Fig. S9, ESI:† (yellow frame) **MMB@NPs-Ru(bpy)$_3^{2+}$** (a) small, (b) medium, (c) large; (green frame) **MMBs@NPs-Ru(bpy)$_2$bps** (d) small, (e) medium, and (f) large. Acquisition conditions: potential 0 V – 2 s and of 1.4 V – 8 s (*vs.* Ag/AgCl), 180 mM TPrA, PB 0.2 M pH 6.9, Pt working electrode, Pt wire as a counter electrode. Integration time 8 s (sensitivity 1200, gain sensitivity 5); magnification 100×; scale bar 3 μm. Right: Histogram representing the ECL signal intensities normalized by the corresponding photoluminescence signals for samples **NPs-Ru(bpy)$_3^{2+}$** (yellow) and **NPs-Ru(bpy)$_2$bps** (green) (SD calculated for $n \geq 3$).

properties of Ru(bpy)$_2$bps (which are similar to Ru(bpy)$_3$), but quite surprisingly to its capability to self-organize within the silica network of the NP close to the boundary between the NP core and the organo-silica functionalized shell. This behavior can be explained by considering the different charge schemes of the complexes. These results provide important indications for the design and optimization of ECL active nanoprobes based on Ru(II) complex-doped silica nanoparticles to obtain higher signal amplifications.

Research funded by MIUR, grant no. 2020CBEYHC (AStraLI), and supported by ECLipse project (European Union's Horizon Europe EIC Pathfinder Open program under grant agreement no. 101046787). Authors would like to thank Prof. Aurore Fraix, University of Catania, Italy for her kind help with NTA measurements.

Data availability

Other data supporting this article have been included as part of the ESI.† Experimental data are also available at AMS Acta at **https://amsacta.unibo.it/id/eprint/7361/**.

Conflicts of interest

There are no conflicts to declare.

Notes and references

1 N. Sojic, *Analytical Electrogenerated Chemiluminescence: From Fundamentals to Bioassays*, The Royal Society of Chemistry, 2019.
2 C. Ma, Y. Cao, X. Gou and J. J. Zhu, *Anal. Chem.*, 2015, **92**, 431–454.
3 A. Zanut, A. Fiorani, S. Canola, T. Saito, N. Ziebart, S. Rapino, S. Rebeccani, A. Barbon, T. Irie, H. P. Josel, F. Negri, M. Marcaccio, M. Windfuhr, K. Imai, G. Valenti and F. Paolucci, *Nat. Commun.*, 2020, **11**, 1–9.
4 N. Myung, X. Lu, K. P. Johnston and A. J. Bard, *Nano Lett.*, 2004, **4**, 183–185.
5 X. Chen, Y. Liu and Q. Ma, *J. Mater. Chem. C*, 2018, **6**, 942–959.
6 Z. Cao, C. Li, Y. Shu, M. Zhu, B. Su, H. Qin and X. Peng, *J. Am. Chem. Soc.*, 2023, **145**, 26425–26434.
7 X. Huang, B. Li, Y. Lu, Y. Liu, S. Wang, N. Sojic, D. Jiang and B. Liu, *Angew. Chem., Int. Ed.*, 2023, **62**, e202215078.
8 A. Zanut, F. Palomba, M. Rossi Scota, S. Rebeccani, M. Marcaccio, D. Genovese, E. Rampazzo, G. Valenti, F. Paolucci and L. Prodi, *Angew. Chem., Int. Ed.*, 2020, **59**, 21858–21863.
9 Y. Liu, H. Zhang, B. Li, J. Liu, D. Jiang, B. Liu and N. Sojic, *J. Am. Chem. Soc.*, 2021, **143**, 17910–17914.
10 F. Arcudi, L. Dordevic, S. Rebeccani, M. Cacioppo, A. Zanut, G. Valenti, F. Paolucci and M. Prato, *Adv. Sci.*, 2021, **8**, 1–9.
11 E. Rampazzo, S. Bonacchi, M. Montalti, L. Prodi and N. Zaccheroni, *J. Am. Chem. Soc.*, 2007, **129**, 14251–14256.
12 L. Wang, C. Lofton, M. Popp and W. Tan, *Bioconjugate Chem.*, 2007, **18**, 610–613.
13 W. Zhu, J. Dong, G. Ruan, Y. Zhou and J. Feng, *Angew. Chem., Int. Ed.*, 2023, **62**, e20221441.
14 G. Valenti, E. Rampazzo, S. Bonacchi, L. Petrizza, M. Marcaccio, M. Montalti, L. Prodi and F. Paolucci, *J. Am. Chem. Soc.*, 2016, **138**, 15935–15942.
15 S. Kesarkar, S. Valente, A. Zanut, F. Palomba, A. Fiorani, M. Marcaccio, E. Rampazzo, G. Valenti, F. Paolucci and L. Prodi, *J. Phys. Chem. C*, 2019, **123**, 5686–5691.
16 A. Reisch, P. Didier, L. Richert, S. Oncul, Y. Arntz, Y. Mély and A. S. Klymchenko, *Nat. Commun.*, 2014, **5**, 1–9.
17 L. Della Ciana, S. Zanarini, R. Perciaccante, E. Marzocchi and G. Valenti, *J. Phys. Chem. C*, 2010, **114**, 3653–3658.
18 F. J. Arriagada and K. Osseo-Asare, *J. Colloid Interface Sci.*, 1995, **170**, 8–17.